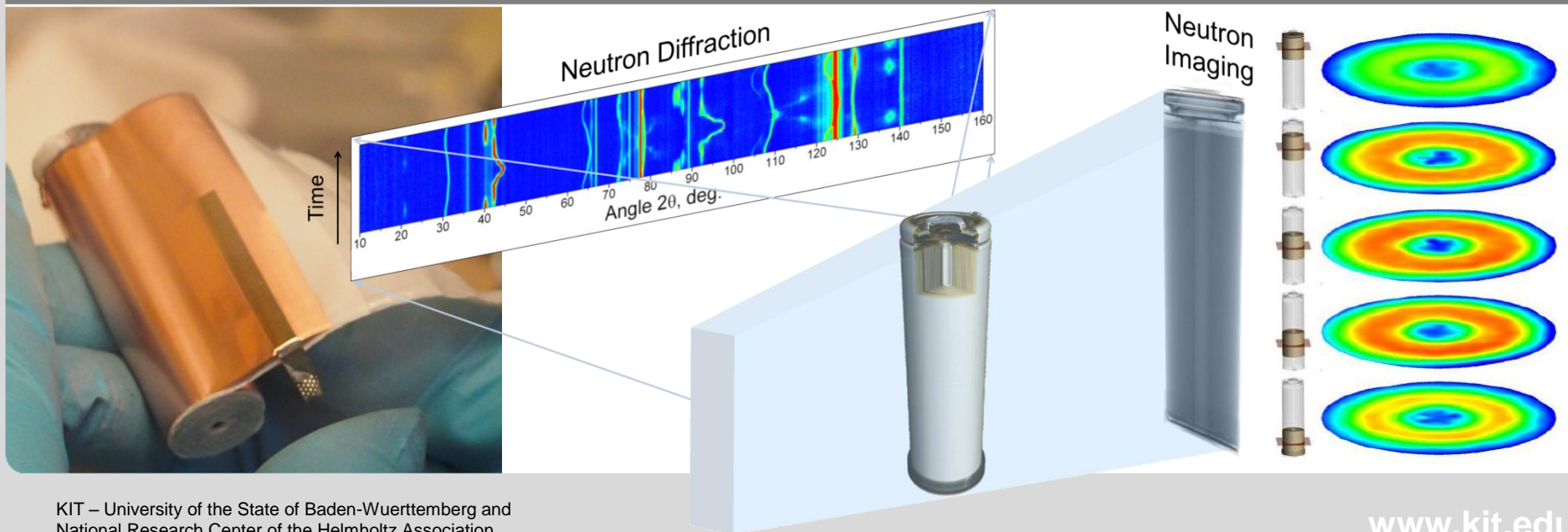


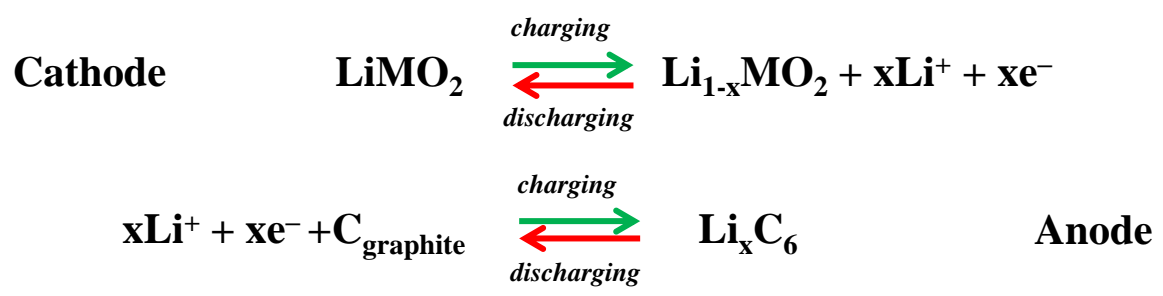
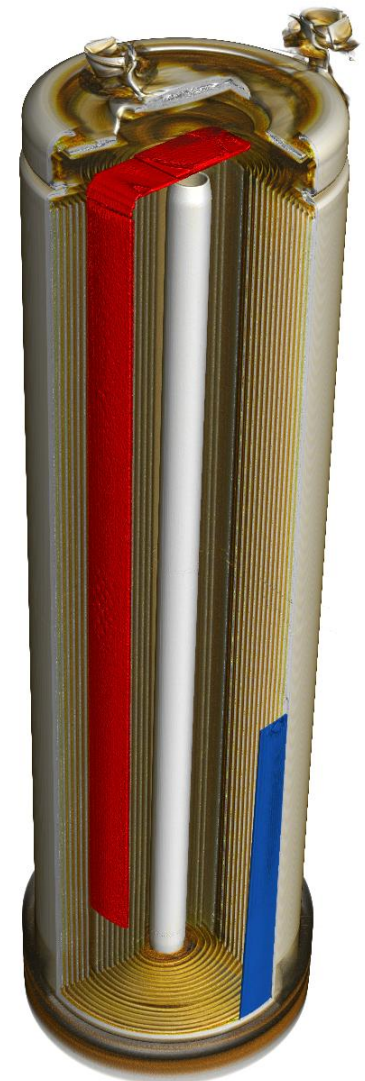
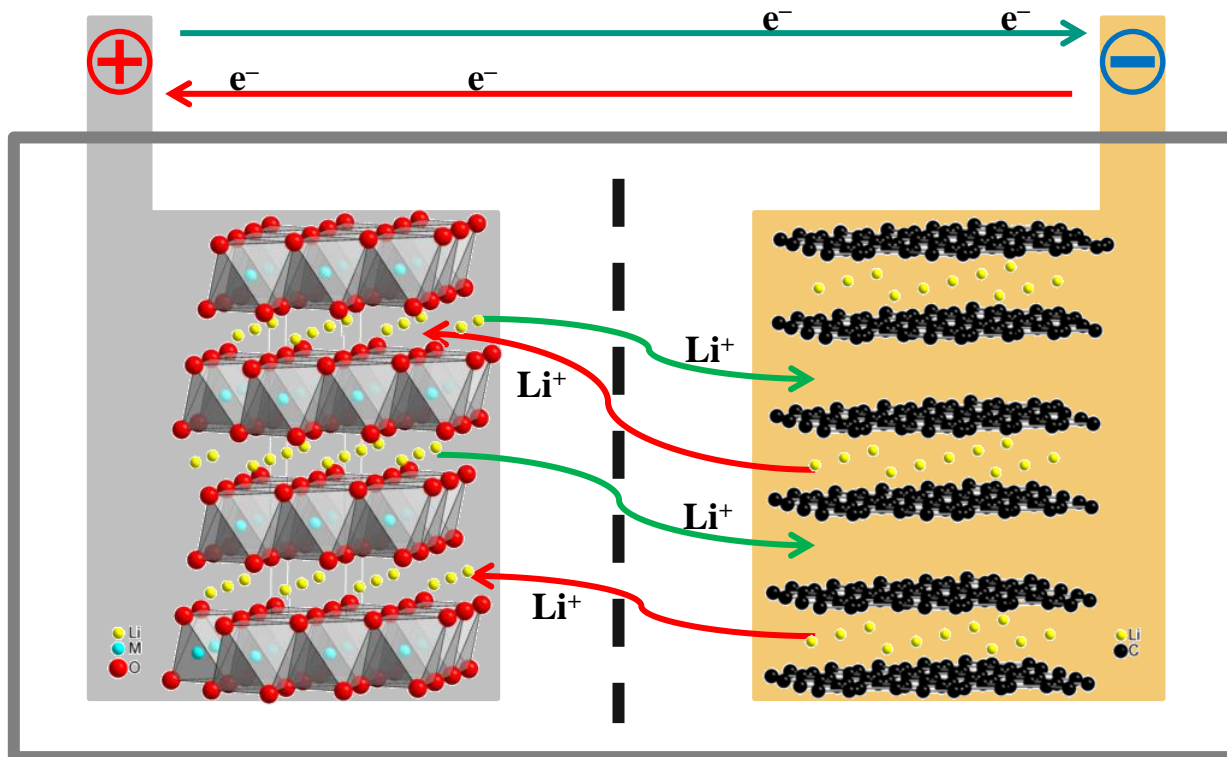
# Uniformity of Lithium-Ion Batteries Probed by Neutron Scattering

M.J. Mühlbauer, Michael Hofmann, Anatoliy Senyshyn

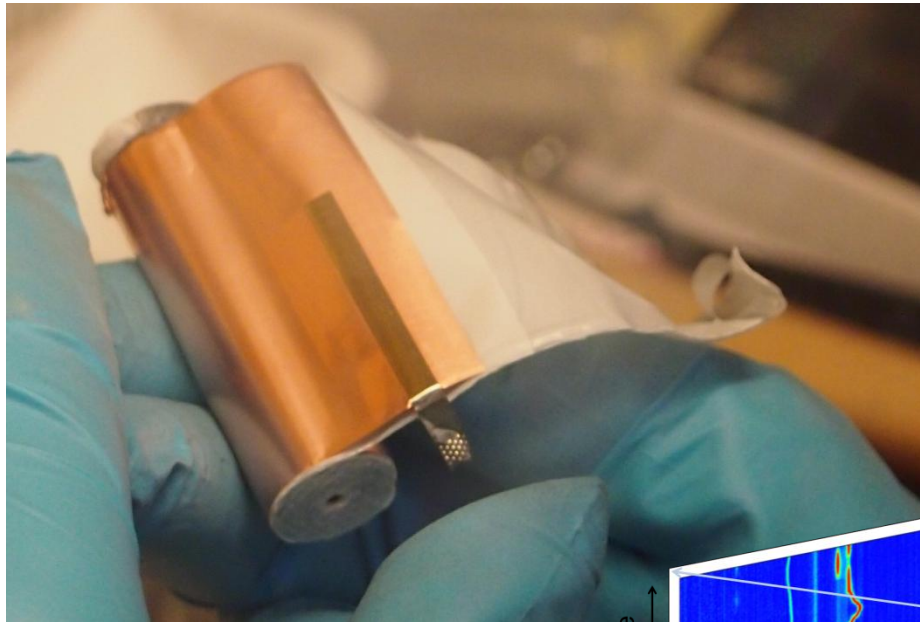
ICNS 2017 - International Conference on Neutron Scattering – Daejeon, Korea



# Schematic of a 18650-type Li-Ion Cell

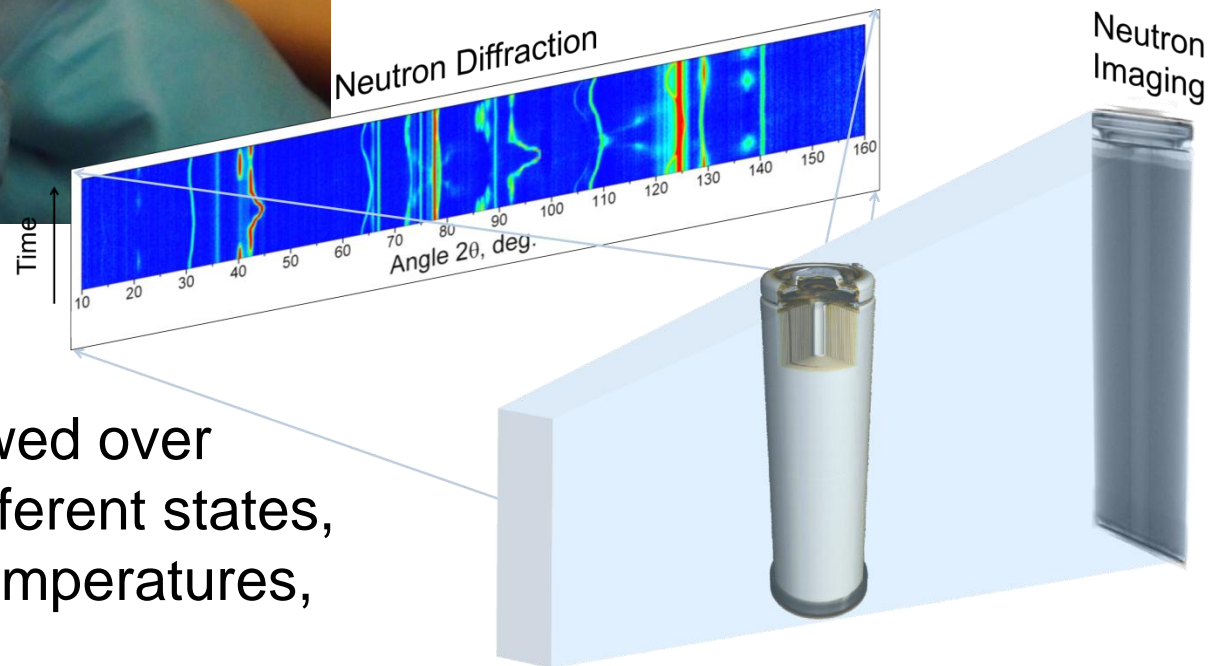


# Why in operando / in situ studies?



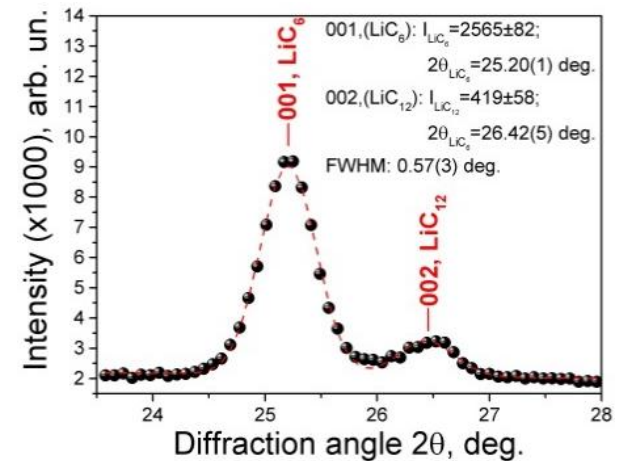
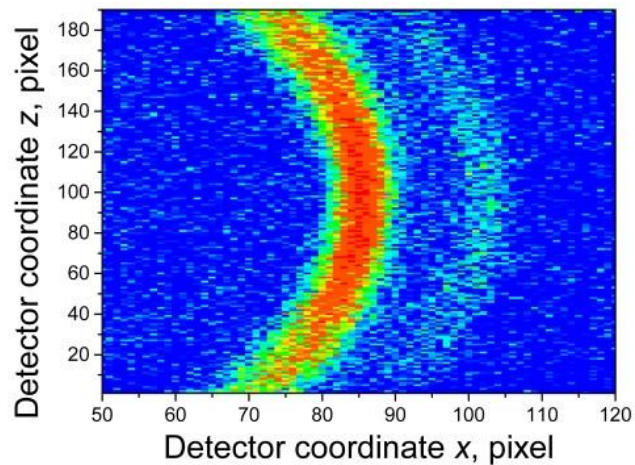
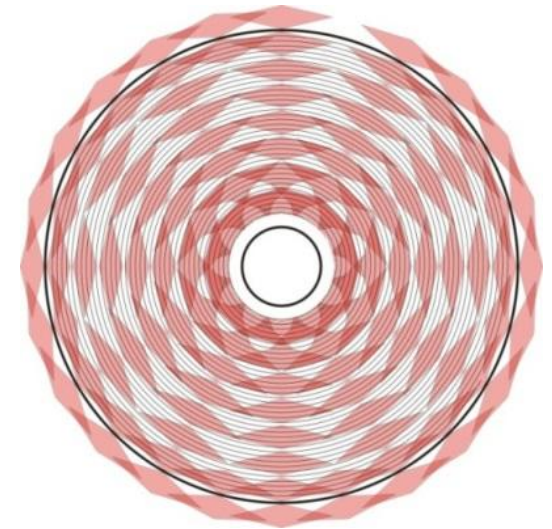
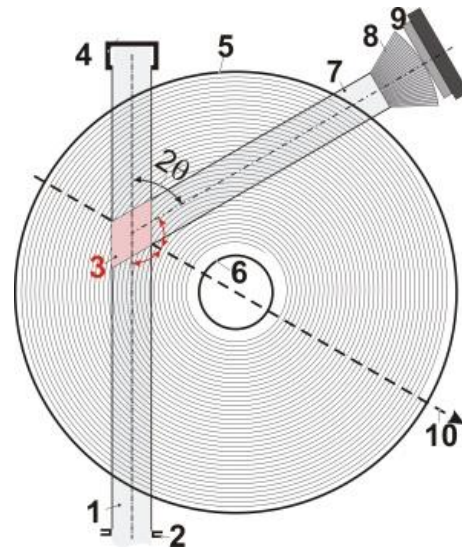
Opening of cells, risk of material changes, e.g. oxidation, short circuits, ...  
 Cells are not available for further studies.

Neutron methods are non-destructive. Cell behaviour is followed over several cycles or at different states, e.g. state of charge, temperatures, fatigue, aging, ...

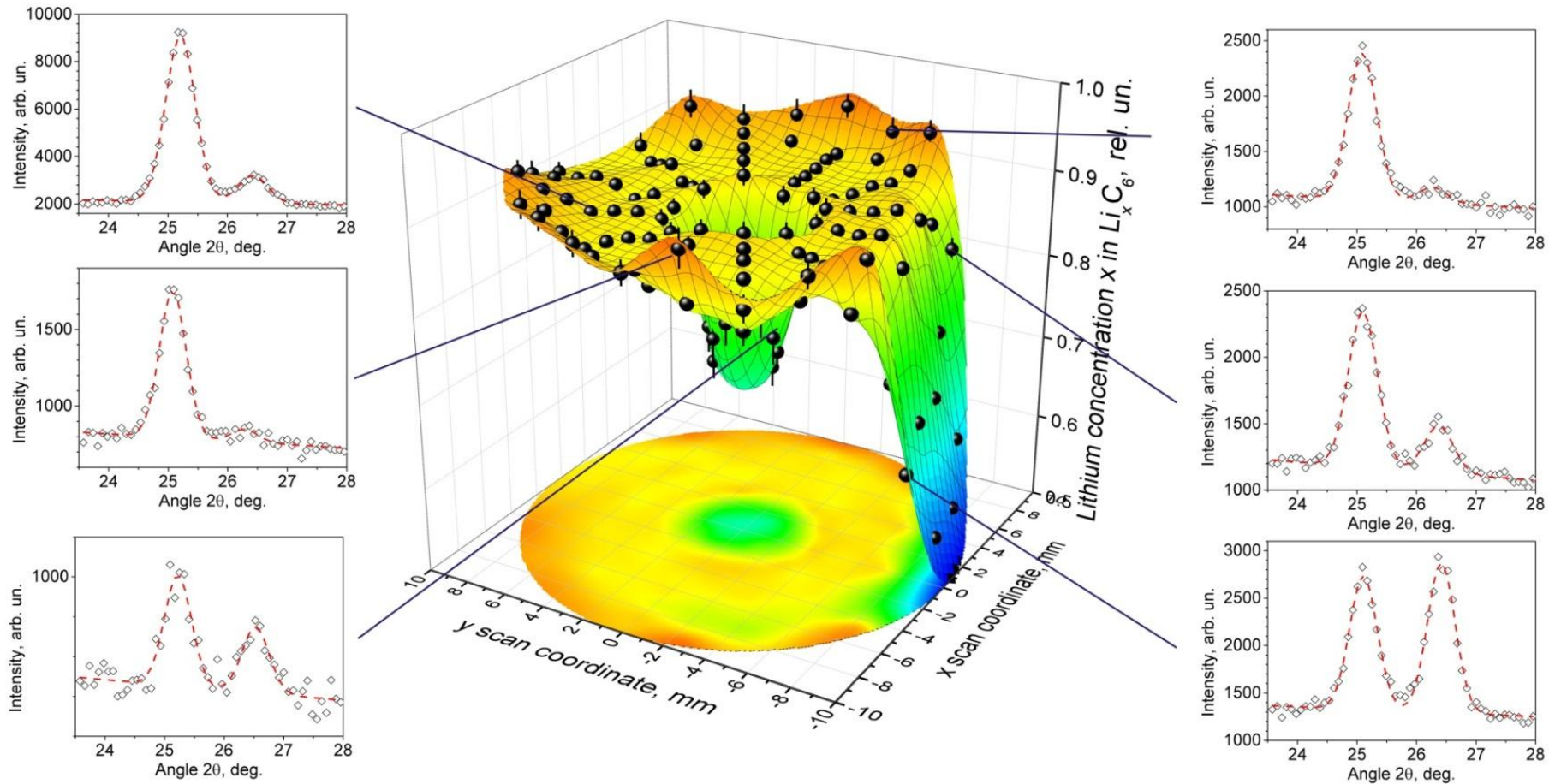




# Spatially Resolved Neutron Diffraction

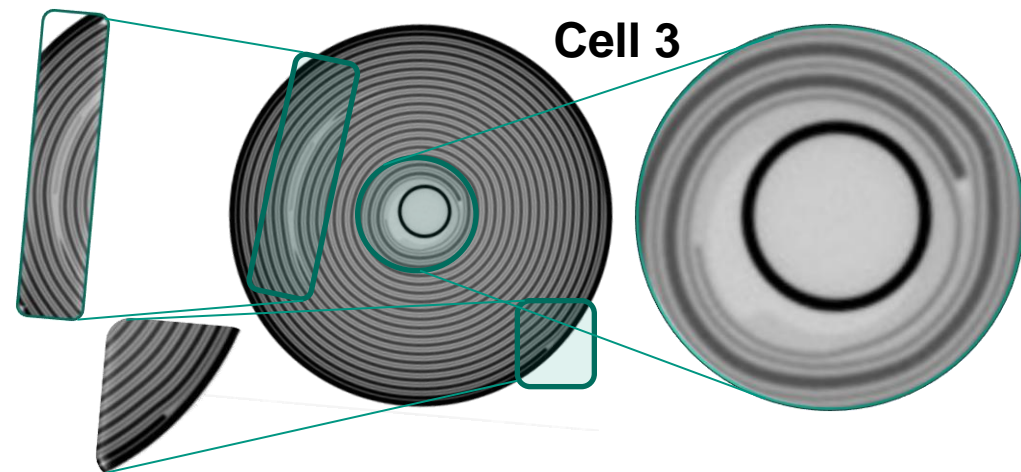
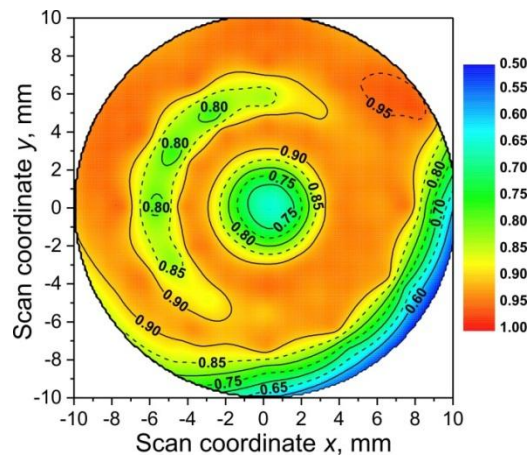
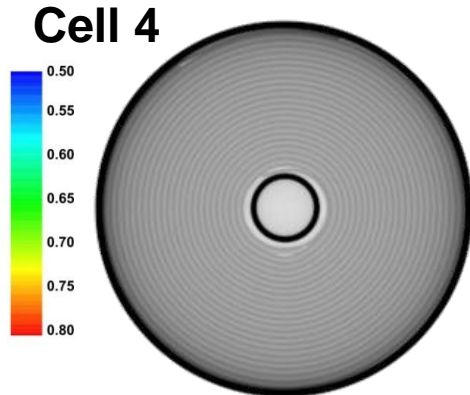
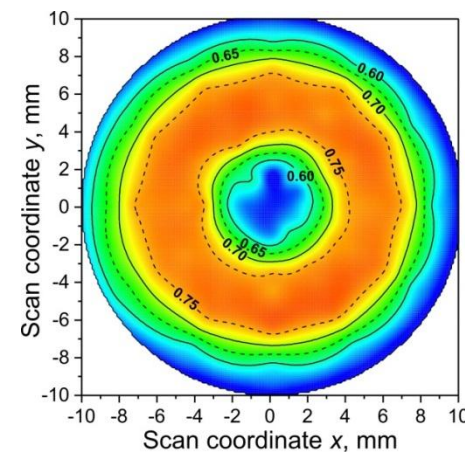
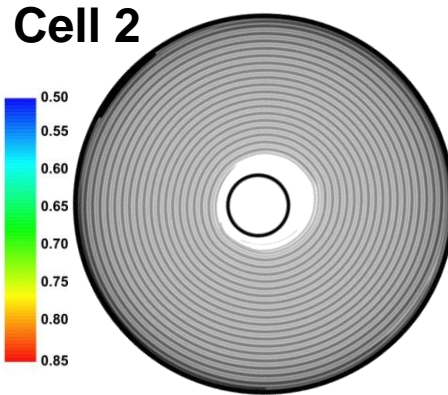
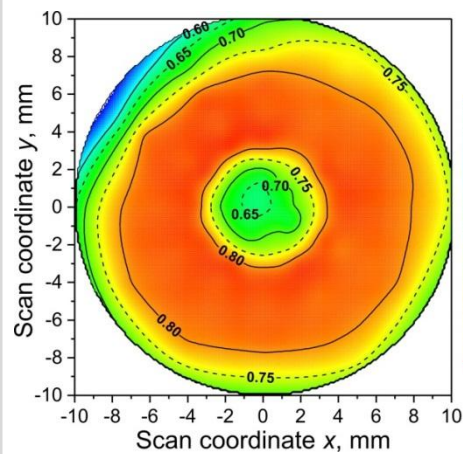


# Lithium Concentration $x$ in $\text{Li}_x\text{C}_6$ , Cell #1

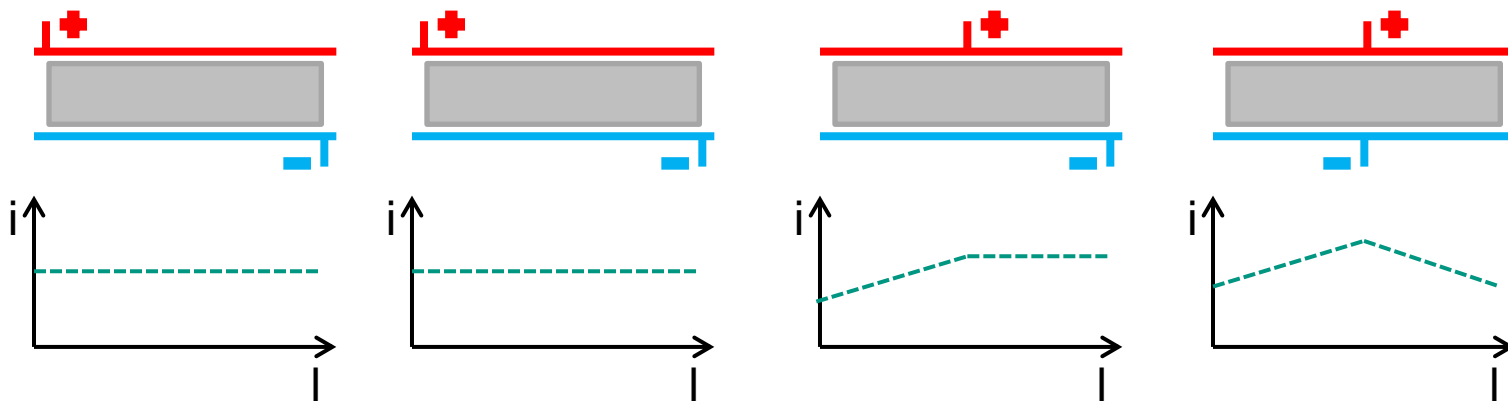
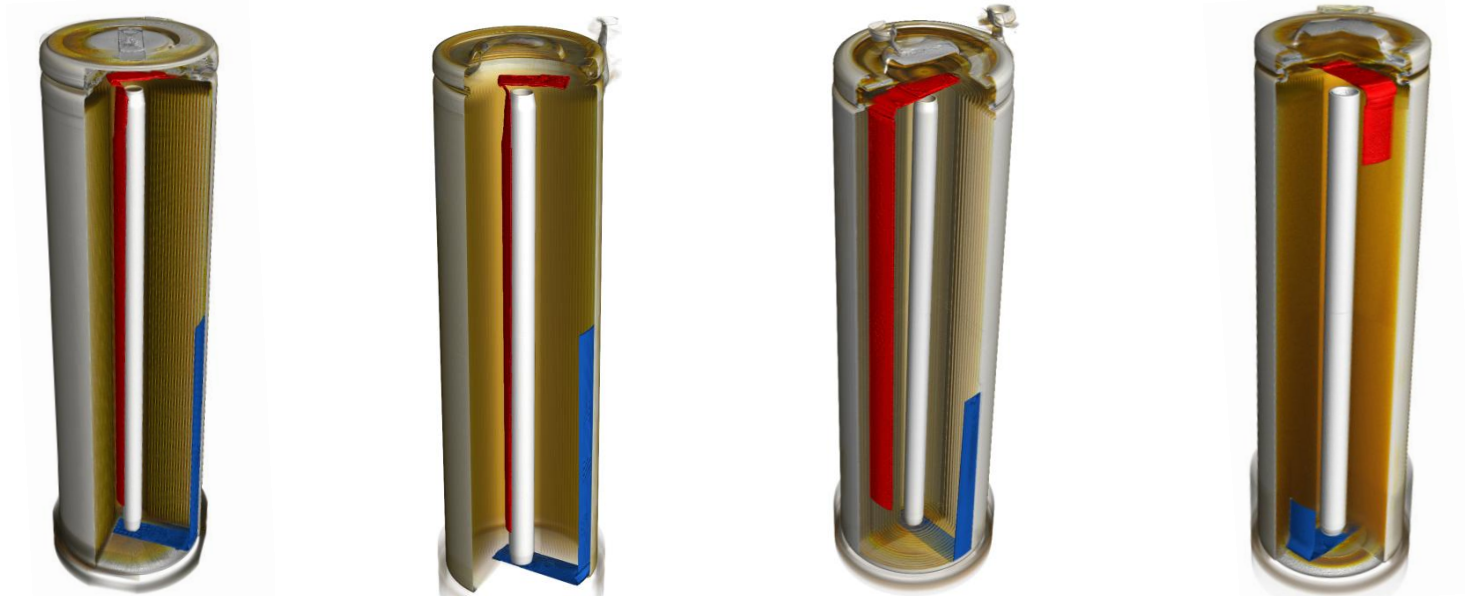




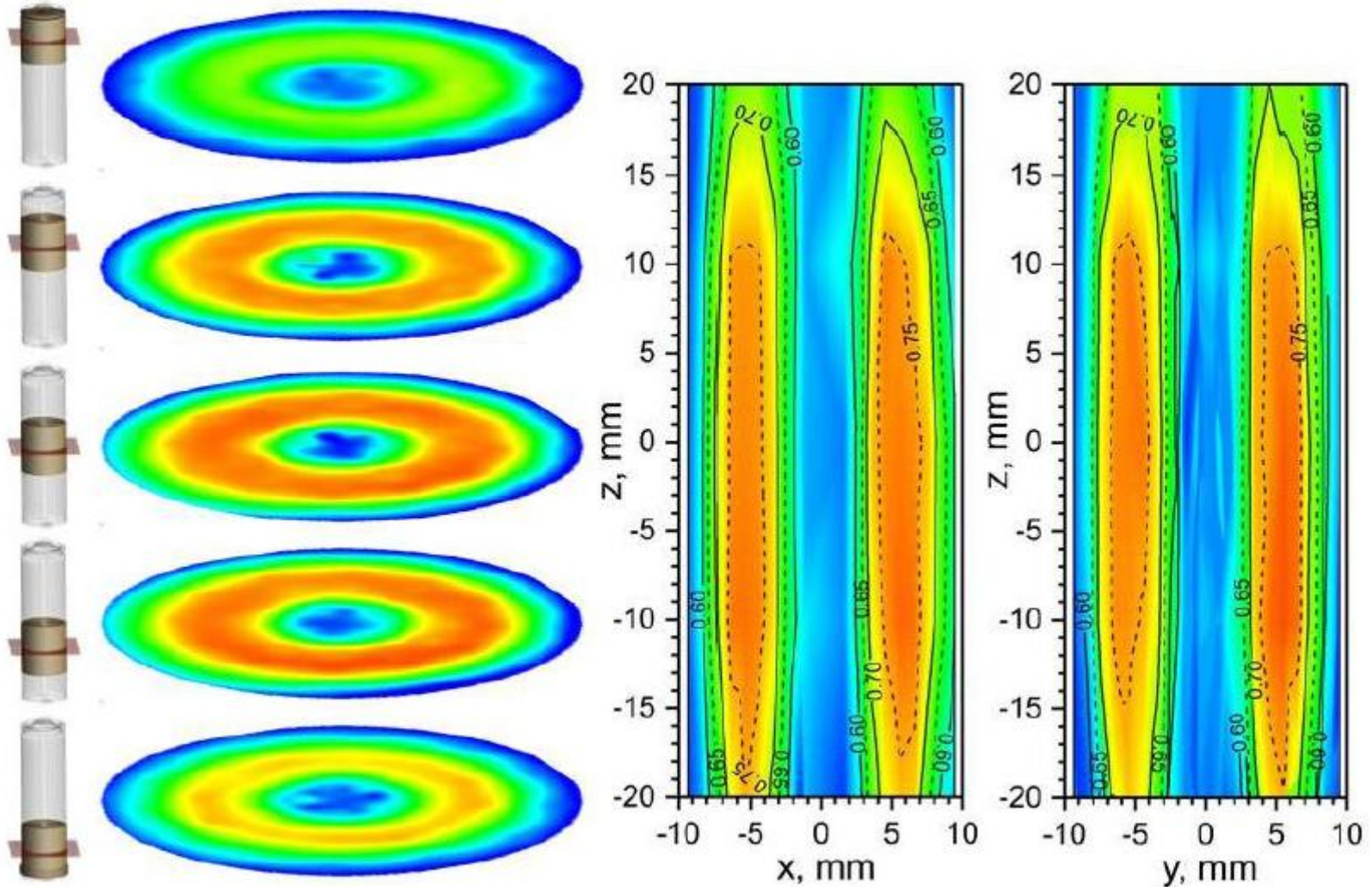
# Lithium Concentration $x$ in $\text{Li}_x\text{C}_6$ , Cells #2 to #4



# Different Cell Geometries → Current Distribution



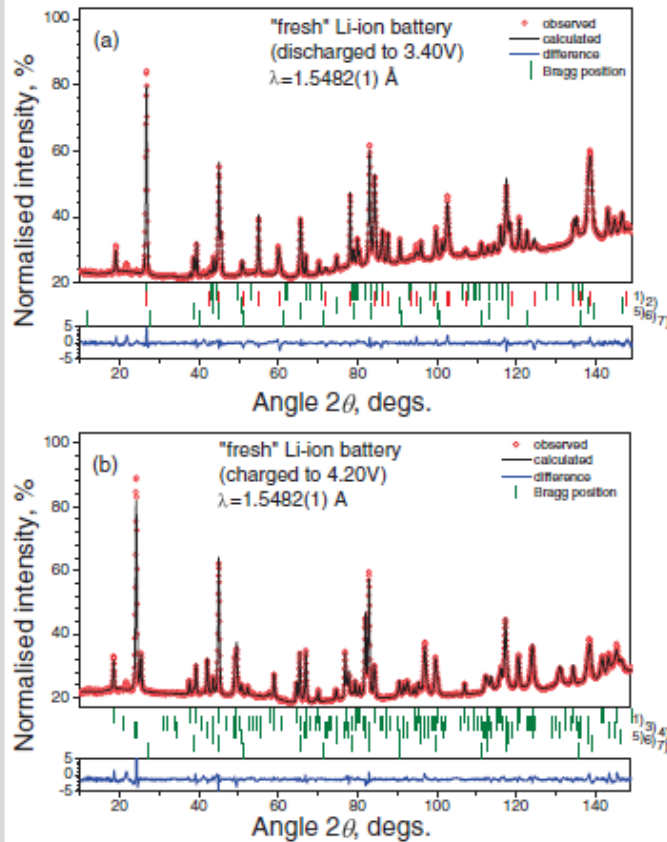
# Non-Uniformity along z-axis



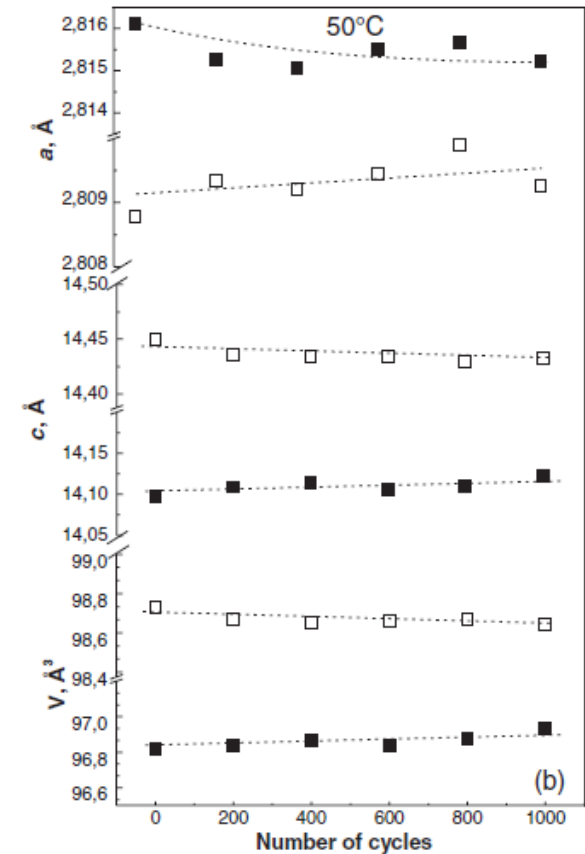
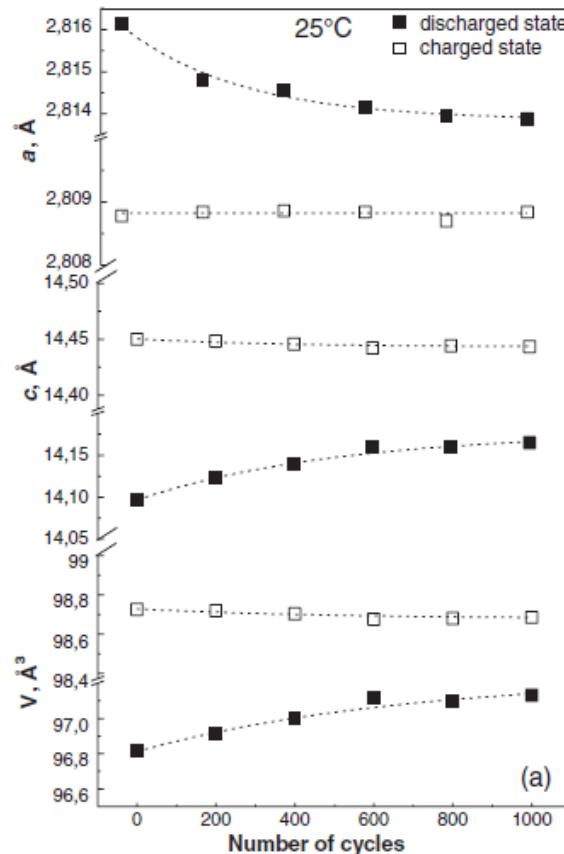


# Investigation of Fatigue in LCO cells

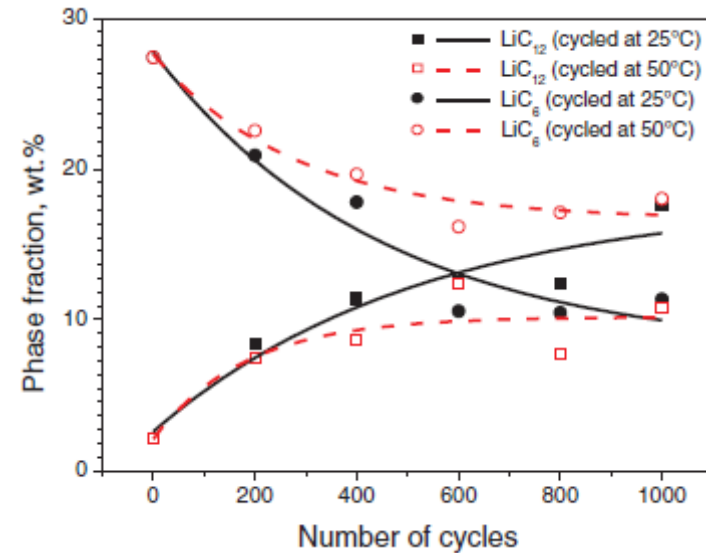
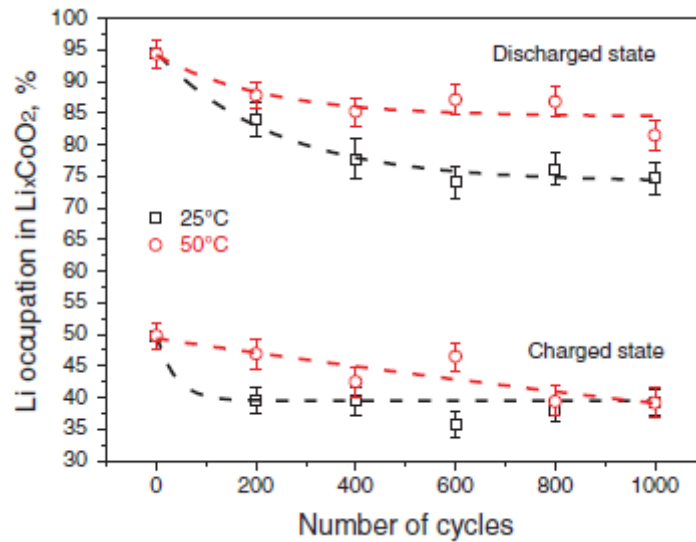
## Rietveld refinement



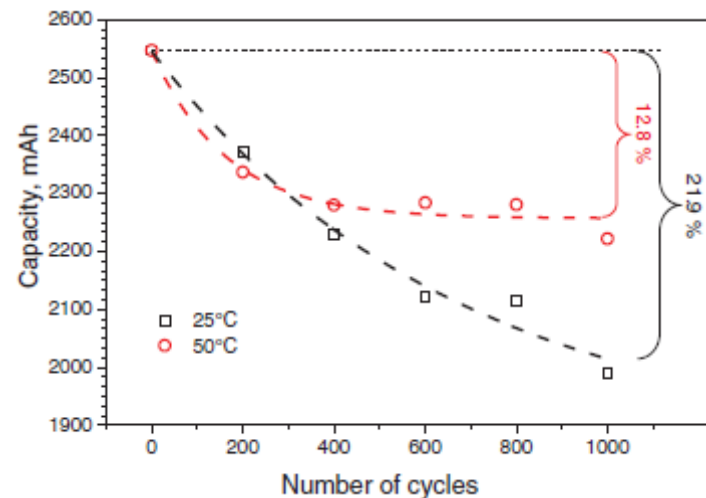
## Lattice parameters and cell volumes



# Investigation of Fatigue in LCO cells



Active Lithium	25°C	50°C
Cathode	21%	12%
Anode	26%	15%



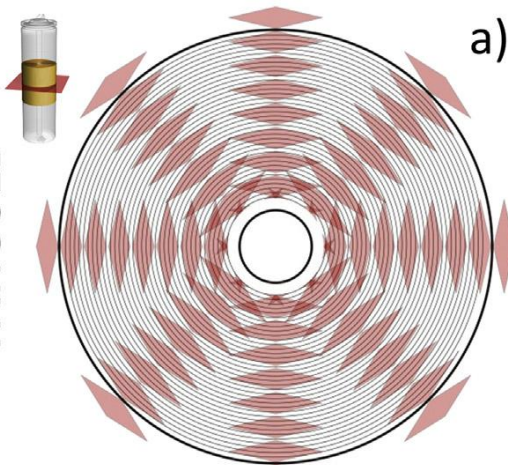
# Effect of Fatigue on Spatial Distribution of Li

Gauge volume configuration

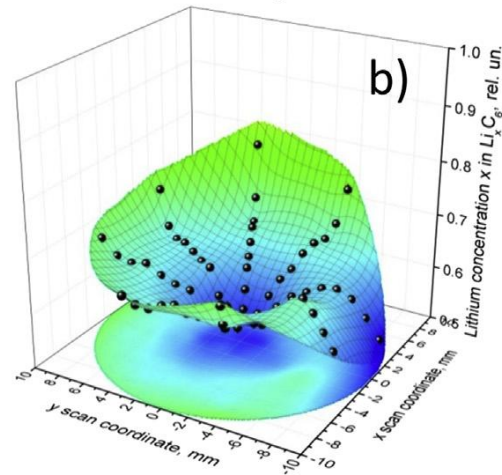
Lithium concentration  $x$  in  $\text{Li}_x\text{C}_6$ , rel. un.  
Surface plot

Contour plot

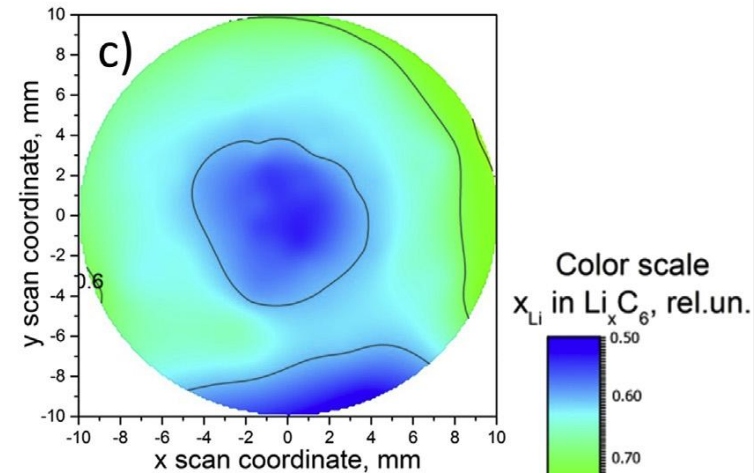
FATIGUED



a)

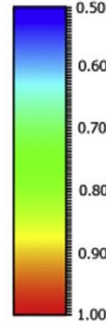


b)

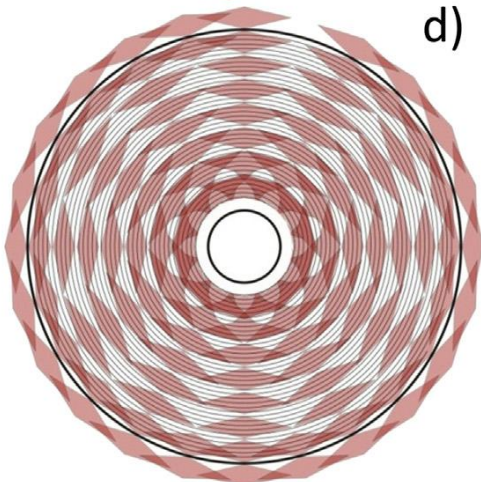


c)

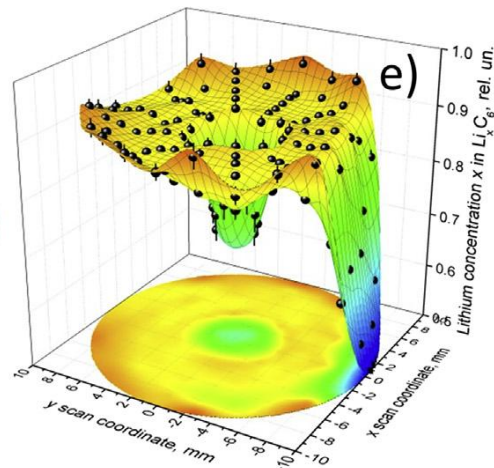
Color scale  
 $x_{\text{Li}}$  in  $\text{Li}_x\text{C}_6$ , rel.un.



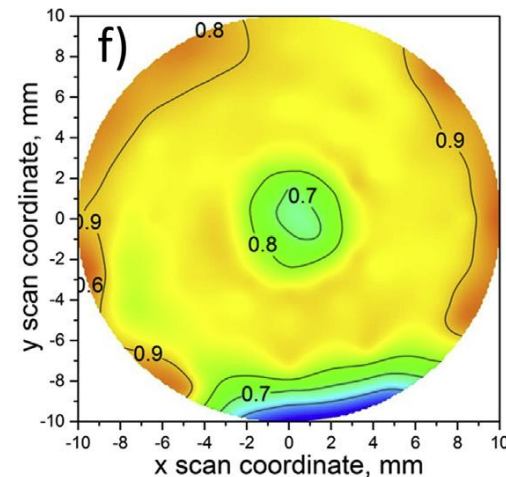
FRESH



d)



e)



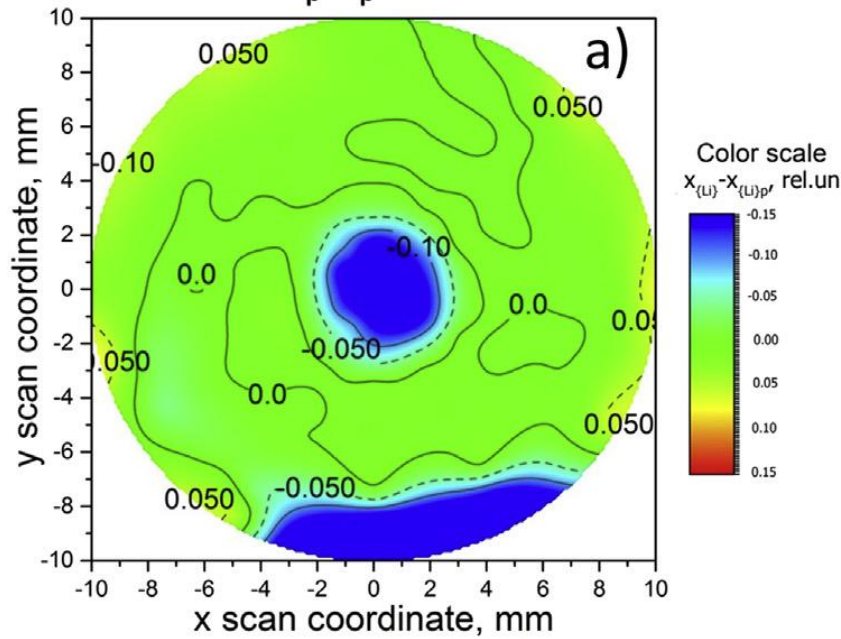
f)



# Deviations from plateau-like distribution

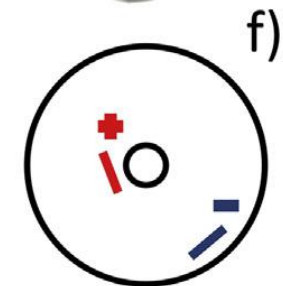
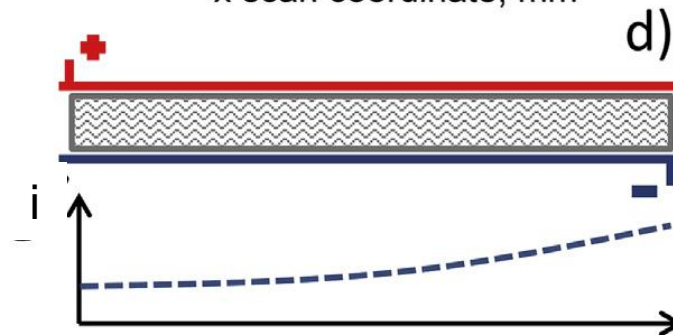
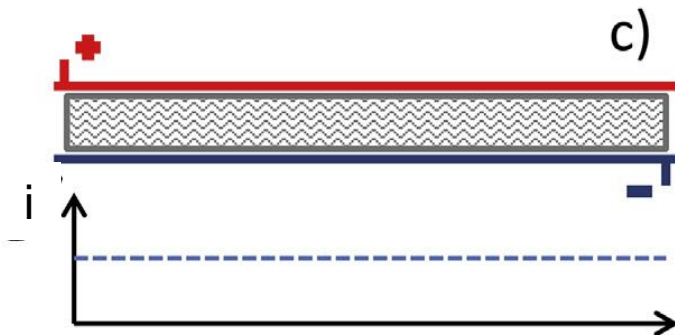
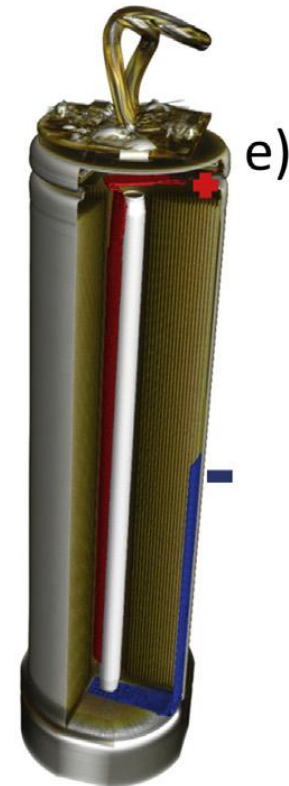
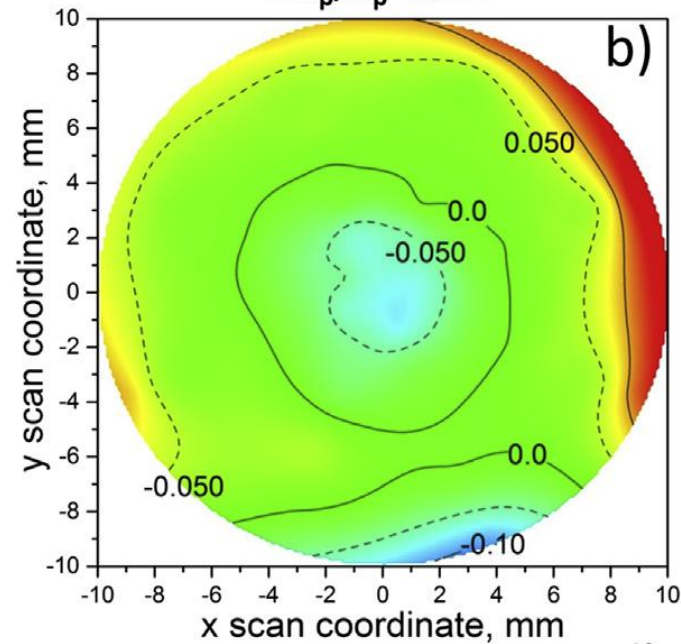
## Fresh cell

$$x - x_p, x_p = 0.88$$



## Fatigued cell

$$x - x_p, x_p = 0.61$$



# ERWIN - 05K16VK2

## “Energy Research with Neutrons”

# NECTAR - 05K16VK3

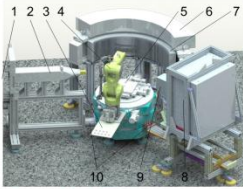
## “Thermische Neutronen am Messplatz NECTAR”



### Neutron Powder Diffraction Option ERWIN at beamport 8b at MLZ

M.J. Mühlbauer<sup>1,2</sup>, M. Heere<sup>2</sup>, M. Knapp<sup>2,3</sup>, B. Pedersen<sup>1</sup>, A. Senyshyn<sup>1</sup>, H. Ehrenberg<sup>2,3</sup>

<sup>1</sup> Heinz Maier-Leibnitz Zentrum (MLZ), <sup>2</sup> Karlsruher Institut für Technologie (KIT), <sup>3</sup> Helmholtz Institute Ulm (HIU)

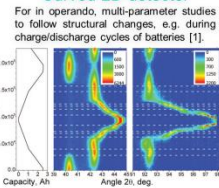


- Instrumentation of ERWIN**
- 1) monochromatic beam exit (incl. PG monochromator)
  - 2) secondary flight path comprising of:
    - i. Fast shutter
    - ii. Collimator changer
    - iii. Filter changer
    - iv. System of slits
    - v. Neutron monitor
    - vi. Optional focusing neutron guide
  - 3) Stack of vanadium sample containers
  - 4) 6 axis robot for changing of samples
  - 5) Sample table (x, y, z,  $\psi$ ,  $\theta$ ,  $\phi$ )
  - 6) Large curved 2D multidetector (r=750 mm, h=200 mm, 2 $\theta$  coverage: 120 – 150 deg.)
  - 7) Radial oscillating collimator
  - 8) Flat 2D neutron detector (500x250mm) for spatially resolved powder diffraction studies
  - 9) Radial oscillating collimator (0.5 mm – 1 mm)
  - 10) fast mechanical remounting plugs

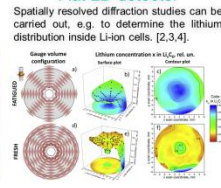
#### Motivation

The need for rapid data collection and studies of small sample volumes in the range of mm<sup>3</sup> are the main driving force for the concept of a high-throughput monochromatic diffraction instrument the Heinz Maier-Leibnitz Zentrum (MLZ). It should address a large section of reciprocal space with sufficient dynamic range and just time-resolution and allow for a variety of different sample environments. The medium-resolution neutron powder diffraction option for “Energy research with neutrons” (ERWIN) at beam port SR8b at MLZ is foreseen to meet the demand. ERWIN will especially be suited for studies on structure and its uniformity of energy-related systems and materials by using simultaneous bulk/spatially resolved neutron powder diffraction. A set of useful experimental options will be implemented enabling time-resolved studies, rapid parametric measurements as a function of external parameters or studies of small samples using an adapted radial collimator. The proposed powder diffraction option ERWIN will bridge the gap in functionality between the high-resolution powder diffractometer SPODI and the time-of-flight diffractometers POWTEX and SAPHIR.

#### Curved 2D detector

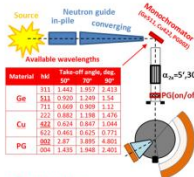


#### Flat 2D detector



#### Simulations

Ray-tracing Monte-Carlo simulations have been performed for the proposed powder option using the existing primary neutron optics monochromator configuration (Ge511 and Cu422) and an additional vertically-focusing pyrolytic graphite monochromator. With this suite of monochromators a broad range of wavelengths (0.46 to 4.8 Å) can be selected from the thermal spectrum at SR8b. Neutron fluxes, divergence profiles and resolution curves were calculated for three configurations: (1) standard-resolution, (2) high-energy and (3) high-intensity mode. The experimental resolution function of the high-resolution diffractometer SPODI is shown for comparison.



#### Summary

- A “fast” powder diffraction option at beamport SR8b is potentially attractive for the user community and it is fairly complementary to the existing and future instrumental pod at the MLZ.
- The location in the “diffractometers corner” of Experimental Hall at the MLZ has a number of advantages regarding transfer of sample environment, equipment and experimental infrastructure.
- The development of a “medium-resolution” powder diffraction using a large 2D detector option will facilitate the research activity in both forms, “internal” and “external”. This helps to consolidate ideas or concepts and to prove them.

#### Acknowledgement

We gratefully acknowledge the funding of the project 05K16VK2 “Energy Research with Neutrons (ERWIN)” by the German Federal Ministry of Education and Research (BMBF).

#### References:

- [1] A. Senyshyn et al. / J. of The Electro. Society 160 (2013)
- [2] A. Senyshyn et al. / Journal of Power Sources 245 (2014)
- [3] A. Senyshyn et al. / Nature Scientific Reports, 5:18380 (2015)
- [4] M.J. Mühlbauer et al. / Journal of Power Sources 348 (2017)



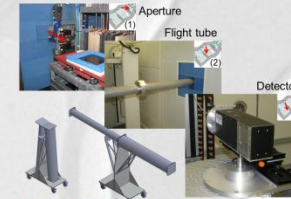
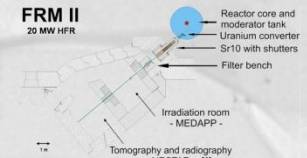
### Neutron Imaging with Fission and Thermal Neutrons at NECTAR at MLZ

M.J. Mühlbauer<sup>1,2,3</sup>, T. Bücherl<sup>4</sup>, M. Knapp<sup>1,2</sup>, M. Makowska<sup>3,5</sup>, M. Schulz<sup>3</sup> H. Ehrenberg<sup>1,2</sup>

<sup>1</sup> Karlsruhe Institut für Technologie (KIT), <sup>2</sup> Helmholtz Institute Ulm (HIU), <sup>3</sup> Heinz Maier-Leibnitz Zentrum (MLZ), <sup>4</sup> Technische Universität München, ZTWB Radiochemie München, <sup>5</sup> University of Bayreuth

#### Motivation

The implementation of a thermal neutron beam option at the NECTAR allows for a combination of thermal and fast neutrons at a single instrument. The thermal beam is accessible by removing the uranium converter and a boron containing filter via remote control requiring only slight modifications of the existing instrumentation. The main components of the instrument like shielding, shutter, access control and sample positioning are kept unchanged. A pure thermal beam extends the neutron energy spectra available for neutron imaging at FRM II / MLZ. Therefore, it increases the flexibility for imaging applications.

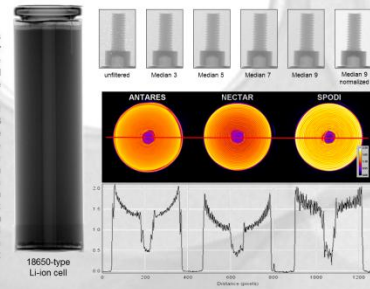


#### Experimental Proof of Concept

(1) An aperture of 25 mm in diameter was installed in front of the filter bench at the neutron beam window of beam tube SR10 and acted as source area for a thermal beam and resulted in a L/D ratio of 240. (2) An evacuated flight tube temporarily installed inside the irradiation room reduced transmission losses for the thermal neutron beam. Borated rubber placed inside the beam tube allowed for cutting the penumbra region of the beam. That way activation of the beam tube and secondary radiation was reduced. (3) A preliminary detector system based on the DELCam [2] including a small rotation stage for tomography. The future flight tube has to be removable to allow for irradiation of patients. A possible layout in operational and storage state is also shown on the left.

#### First Results

The thermal neutron flux at the NECTAR sample position was determined by gold foil activation to be  $7.92 \cdot 10^6 \text{ n} \cdot \text{cm}^{-2} \cdot \text{s}^{-1}$  for an average wavelength of 1.81 Å. Taking into account that the field of view was only limited to 85 mm in diameter by the small flight tube, the thermal neutron beam option does fulfill the requirements of a state of the art neutron imaging facility [3]. There is a large number of gamma spots found for unfiltered data, which can efficiently be removed by filtering a series of 3 to 5 radiographs (images of MS screw on the right). The shielding of the final detector has to be improved and the gamma background at the detector should be reduced. Neutron tomography data have been acquired of a 18650-type Li-Ion cell. A comparison of the thermal data (NECTAR) with data acquired at a cold-thermal beam (ANTARES) shows that beam hardening could be reduced [4]. A larger integral neutron flux results in better signal statistics than for a monochromatic beam  $I = 1.548 \text{ Å}$  (SPODI). The pure thermal neutron beam is a good compromise for larger samples or samples with high neutron absorption, e.g. lithium-ion batteries. Sample activation is kept low, as there is less contribution of cold neutrons.



#### Future Applications

The primary aim of the thermal neutron beam option at NECTAR is its application for energy storage applications, e.g. Li-Ion batteries and related battery systems or hydrogen storage systems. “Dual energy” experiments combining thermal and fast neutron imaging data are a unique feature made possible by the thermal neutron beam option. Besides the use for imaging experiments both neutron spectra will be available for irradiation and activation of samples. The large energy range accessible and multiple filter options at NECTAR also offer an environment for other applications, e.g. detector development, where detection efficiency and sensitivity for background can be tested for two quite different neutron energy spectra, or test of shielding materials, where radiation damage might be of major interest.

We gratefully acknowledge the funding of the project 05K16VK3 “Thermische Neutronen am Messplatz NECTAR” by the German Federal Ministry of Education and Research (BMBF).

- References:
- [1] T. Bücherl et al., NIM A 651 (2011) 86-89.
  - [2] M.J. Mühlbauer et al., NIM A 542 (2005) 324-328.
  - [3] E.H. Lehmann et al., NIM A 651 (2011) 1-5.
  - [4] M.J. Mühlbauer et al., Physics Procedia 88 (2017) 148-153



# Conclusions / Summary

- Overall effects of fatigue and aging can be determined when averaging over the whole cell volume. Changes of:
  - Lattice parameters
  - Li-occupation
  - Phase fractions
- Focusing on partial volumes reveals non-uniform behaviour:
  - Cell geometry / layout, e.g. position of contacts
  - Li-distribution correlated to current distribution
- Change of activity areas inside the cells due to aging/fatigue:
  - In general reduction of active lithium, i.e. change of  $x$  in  $\text{Li}_x\text{C}_6$
  - Areas of largest Li exchange differ for fresh and fatigued cells.





Federal Ministry  
of Education  
and Research

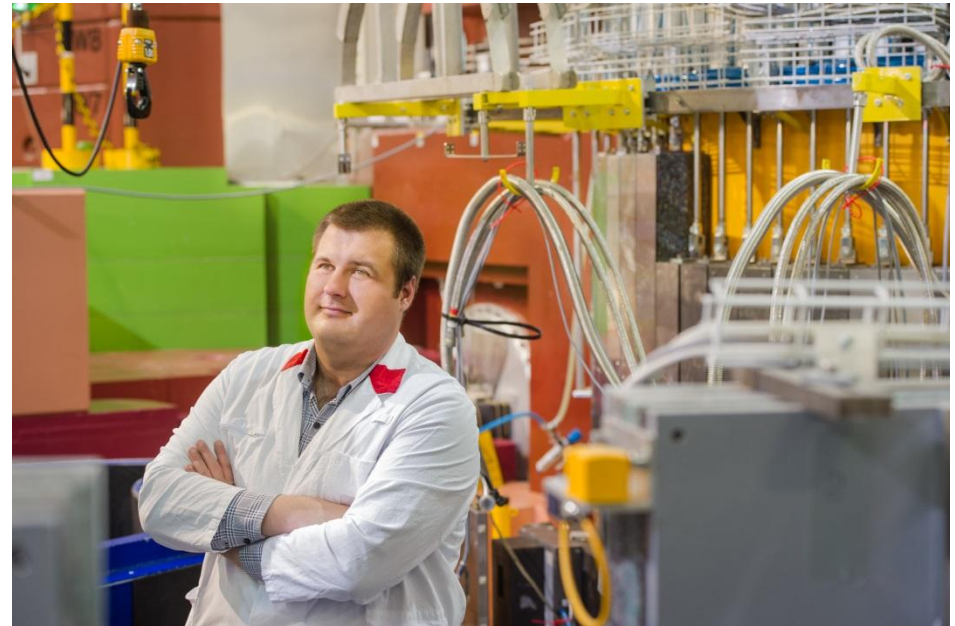
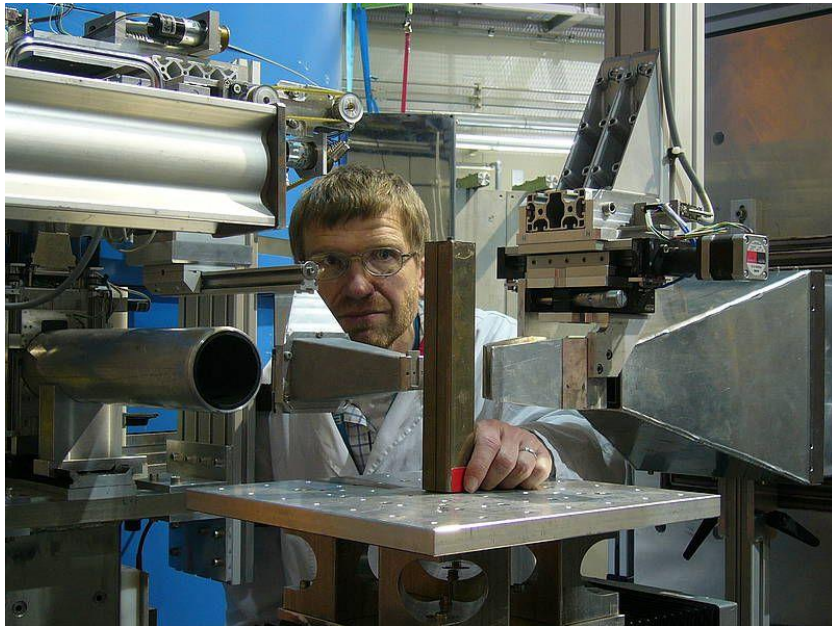


Helmut Ehrenberg

Michael Hofmann

Michael Knapp

Anatoliy Senyshyn



Thanks for Your Attention



# Spatially Resolved Neutron Diffraction

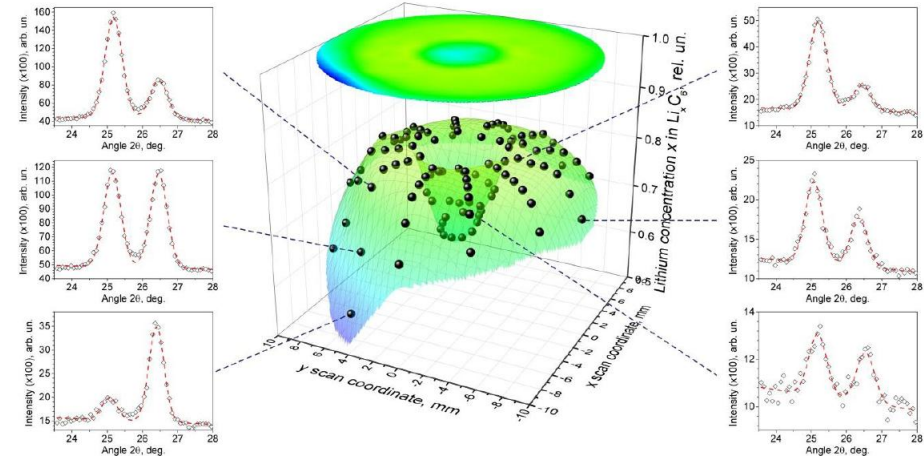
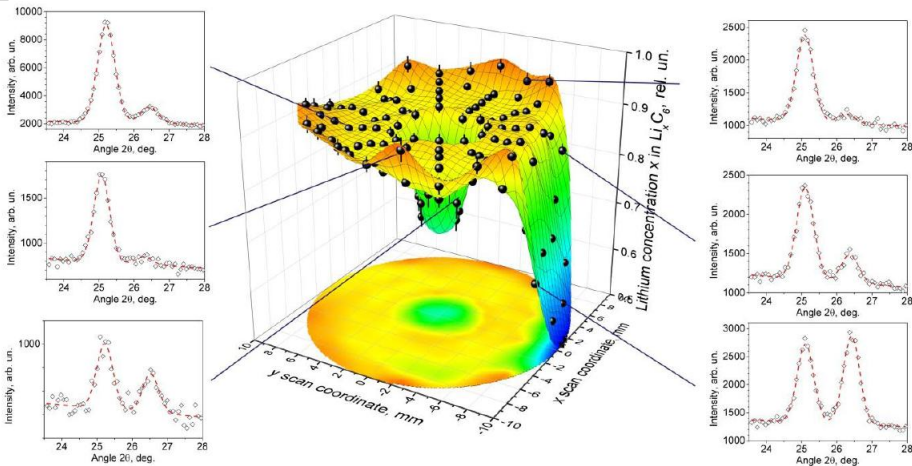


Fig. S2. Spatial distribution of mean lithium concentration in cell 1. Experimental data are shown by black points and surfaces in false color representation (similar to ones the used in Figs. 2) display the interpolation results. Insets illustrate obtained diffraction data at selected coordinates.

Fig. S3. Spatial distribution of mean lithium concentration in cell 2. Experimental data are shown by black points and surfaces in false color representation (similar to ones the used in Figs. 2) display the interpolation results. Insets illustrate obtained diffraction data at selected coordinates.

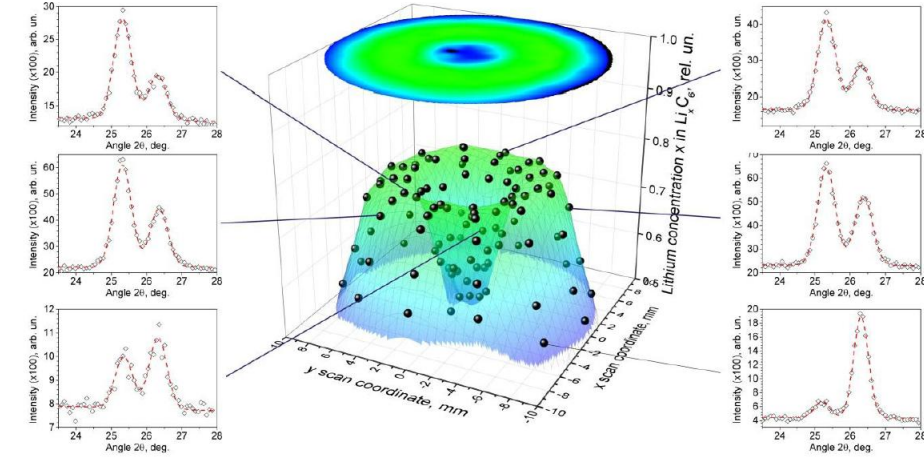
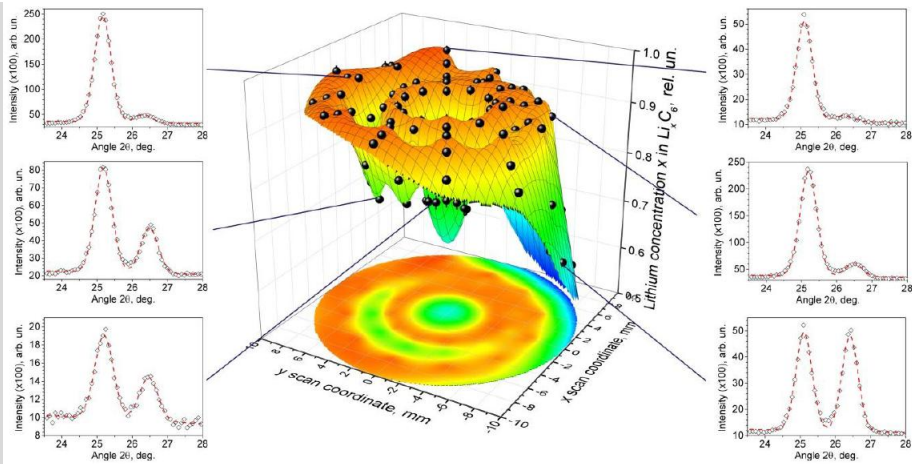


Fig. S4. Spatial distribution of mean lithium concentration in cell 3. Experimental data are shown by black points and surfaces in false color representation (similar to ones the used in Figs. 2) display the interpolation results. Insets illustrate obtained diffraction data at selected coordinates.

Fig. S5. Spatial distribution of mean lithium concentration in cell 4. Experimental data are shown by black points and surfaces in false color representation (similar to ones the used in Figs. 2) display the interpolation results. Insets illustrate obtained diffraction data at selected coordinates.



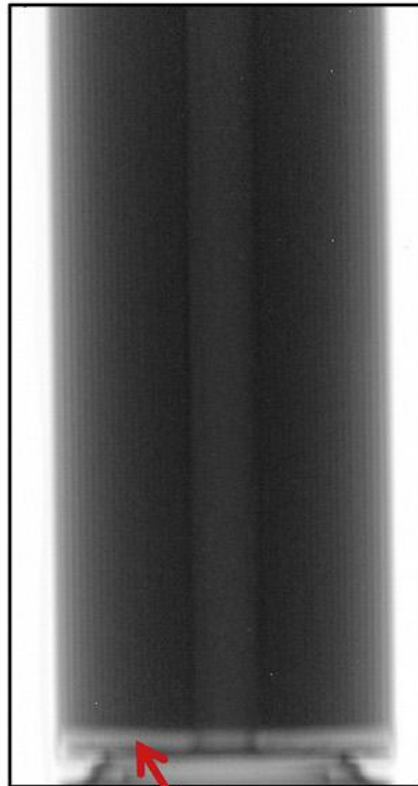
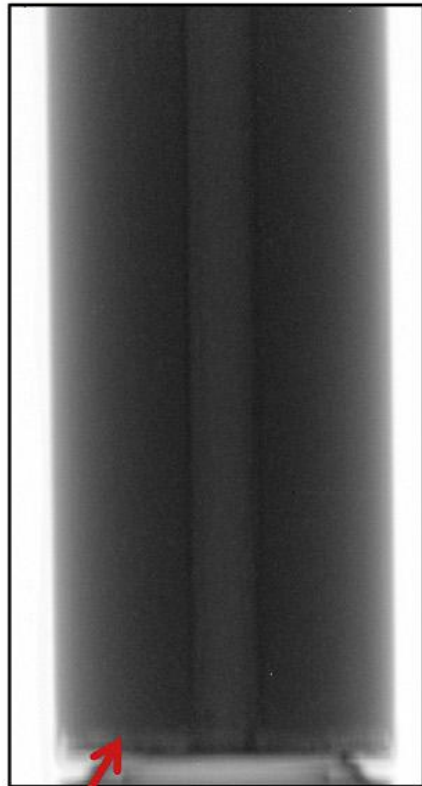
# Level of electrolyte in fresh and fatigued cells



## Fresh cell

charged

discharged



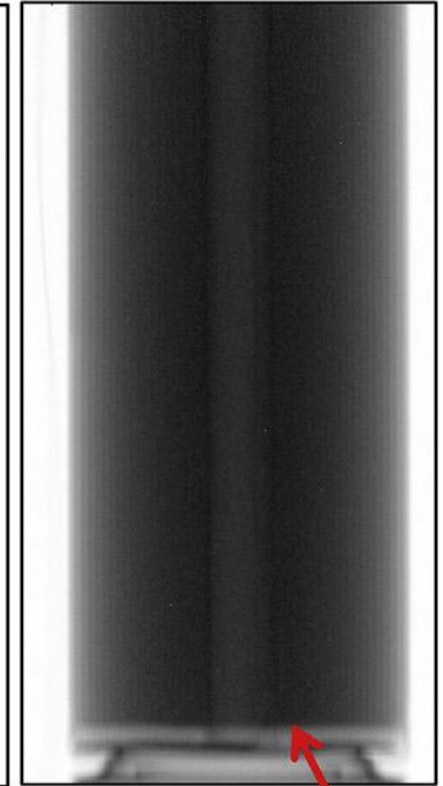
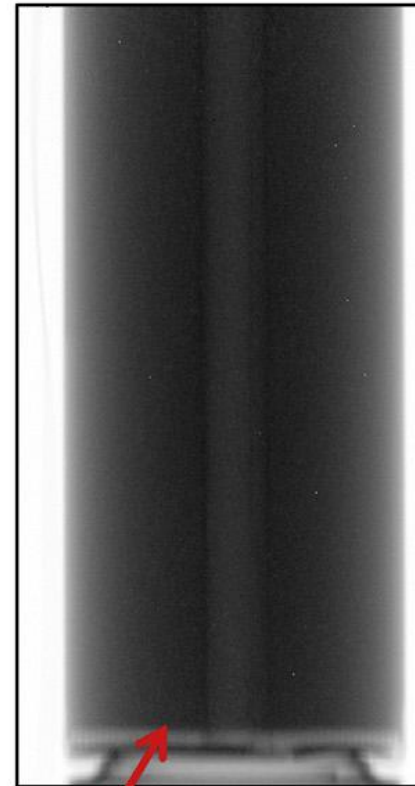
filled

“empty”

## Fatigued cell

charged

discharged



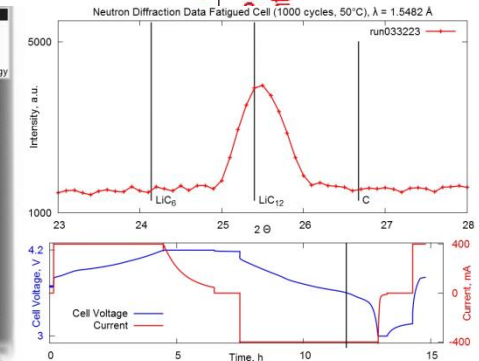
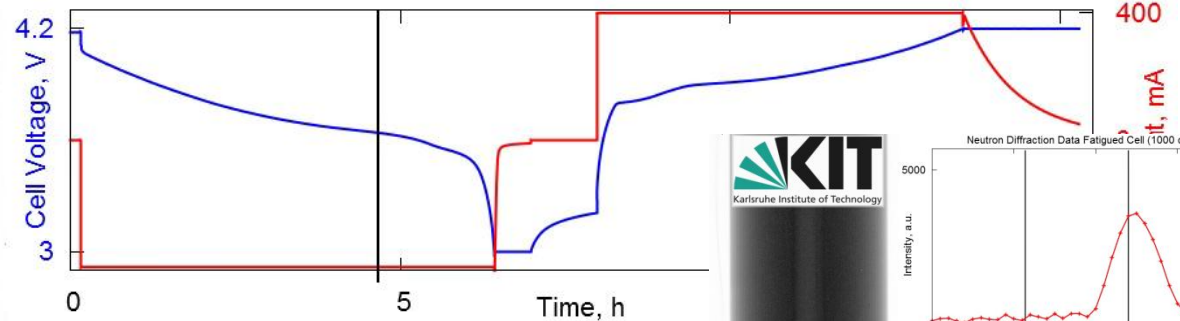
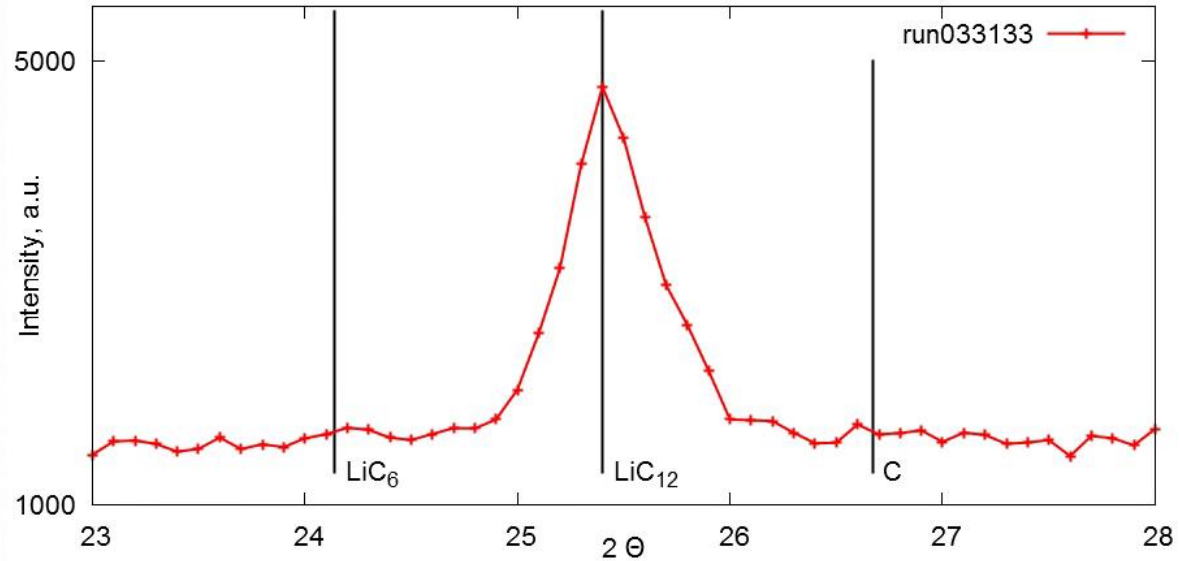
partially empty

“empty”

# Video of electrolyte movement during cycling



Neutron Diffraction Data Fresh Cell,  $\lambda = 1.5482 \text{ \AA}$



Online @ KIT: **“Battery at work, Li-Ionen Batterie”**  
[https://www.youtube.com/watch?v=ICPzHO\\_1nQ8](https://www.youtube.com/watch?v=ICPzHO_1nQ8)